Earth-Science Reviews 207 (2020) 103253

Contents lists available at ScienceDirect

Earth-Science Reviews

journal homepage: www.elsevier.com/locate/earscirev

Melting of a hydrous peridotite mantle source under the Emeishan large igneous province

Rong Xu[a], Yongsheng Liu[a,*], Sarah Lambart[b]

[a] State Key Laboratory of Geological Processes and Mineral Resources, School of Earth Sciences, China University of Geosciences, Wuhan 430074, China
[b] Department of Geology and Geophysics, University of Utah, Salt Lake City, UT, United States

ARTICLE INFO

Keywords:
Mantle plume
Peridotite
Pyroxenite
Olivine composition
Melt inclusion

ABSTRACT

Large igneous provinces on Earth result from anomalously enormous volcanic eruptions at high melt production rates. These eruptions are often linked to catastrophic events such as mass extinctions, global climate changes, or continental break-up. Decoding their petrogenesis is therefore of great importance for our comprehensive understanding of the evolution and geodynamics of our planet. The ~260 Ma Emeishan large igneous province is an important geological feature of SW China with world-class ore deposits and is also suggested to be linked with the Capitanian mass extinction. However, fundamental aspects of the genesis of Emeishan province's most primitive lavas (picrites), such as the source lithology (pyroxenite or peridotite), the origin of compositional variations of olivines and the melting temperature and pressure conditions, remain poorly constrained. Here, we compile information on melt inclusion and host olivine, and whole-rock compositions from the ELIP picrites and show that these data are consistent with decompression melting of a relatively homogeneous peridotitic mantle plume, with a potential temperature higher than 1560 °C. The compositional variability of the olivines and picrites can be explained by varying the equilibrium depth of primary magma segregation and does not require the contribution of a pyroxenite component as previously suggested. Our results favor a scenario for the origin of the Emeishan large igneous province in which the decompression melting during upwelling of a hot hydrous and oxidized mantle plume is accompanied by catastrophic lithospheric thinning. In combination with the now extensive multi-element geochemical data, our findings provide a starting point for re-evaluation of the petrogenesis models for large igneous provinces.

1. Introduction

The formation of the Phanerozoic large igneous province (LIP), contemporaneous with mass extinctions (Ernst and Youbi, 2017; Shellnutt, 2014; Xu et al., 2004), is often ascribed to the presence of a thermal mantle plume that originated in the mantle or at the core-mantle boundary (Anderson, 2005; Campbell, 2007; Chung and Jahn, 1995; Herzberg et al., 2007). Additionally, during the last several decades, evidence from trace elements and isotopes corroborate that the mantle sources of LIPs are highly heterogeneous (Ernst, 2014; Heinonen et al., 2014; Sobolev et al., 2007; Xiao et al., 2004). While the presence of chemical heterogeneity and contribution of recycled crustal material to the magma genesis are overall accepted, there is no consensus on the lithologic nature of the heterogeneity (i.e., peridotite vs. pyroxenites). The high Ni contents and Fe/Mn ratios measured in olivine phenocrysts have been interpreted as reflecting the contribution of a pyroxenite component (Herzberg, 2011; Kamenetsky et al., 2012; Ren et al., 2017; Sobolev et al., 2007). However, several recent studies challenged this interpretation and suggested that variations of melting conditions of a peridotite source are sufficient to explain the compositional range of olivine phenocrysts from LIPs (Heinonen and Fusswinkel, 2017; Matzen et al., 2013; Matzen et al., 2017b; Niu et al., 2011; Putirka et al., 2011).

At a given pressure, most pyroxenites have lower melting temperatures and higher melt productivities than peridotites (Hirschmann et al., 2003; Kogiso, 2004; Lambart et al., 2016; Lambart et al., 2013). Hence, for a same volume of magma, a mantle source containing a pyroxenite component could produce melts with a chemical signature reflecting a higher melting degree than expected for a homogeneous peridotitic source (e.g., Lambart, 2017; Stolper and Asimow, 2007). Therefore, calculations of mantle melting conditions from primary magma compositions without considering the source lithology would result in incorrect estimations of the pressure and temperature of melting. Hence, the determination of the source lithology is crucial for a

---

[*] Corresponding author.
E-mail addresses: rongxu@cug.edu.cn (R. Xu), yshliu@cug.edu.cn (Y. Liu), sarah.lambart@utah.edu (S. Lambart).

https://doi.org/10.1016/j.earscirev.2020.103253
Received 23 March 2020; Received in revised form 10 June 2020; Accepted 15 June 2020

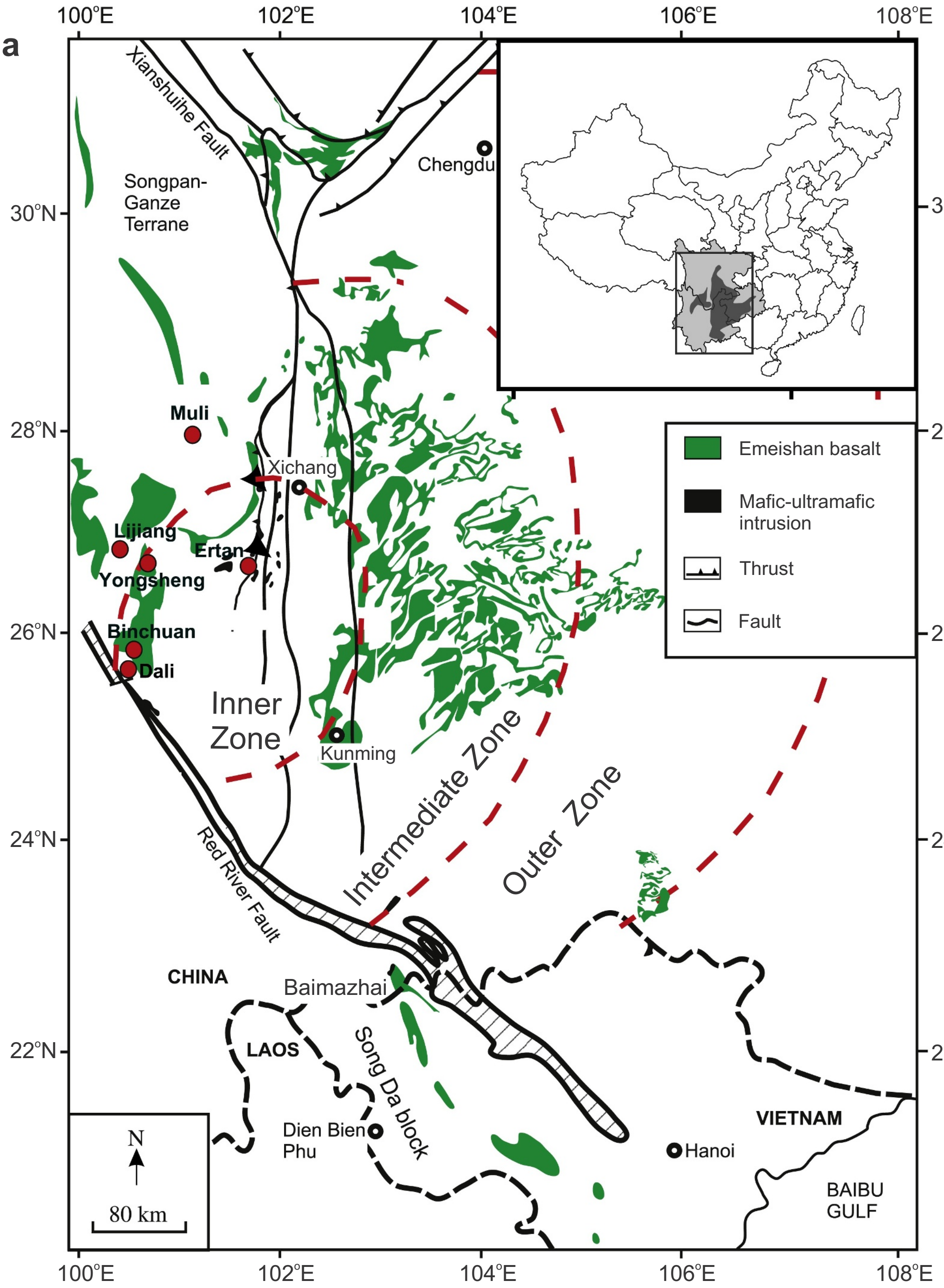

Fig. 1. Distribution and location of the Emeishan large igneous province (modified from Shellnutt (2014)). Red solid circles show locations of picrites. (For interpretation of the references to colour in this figure legend, the reader is referred to the web version of this article.)

comprehensive understanding of the LIP formation.

If the mantle source lithology of the parental melt is constrained to be a peridotite source, the genetic conditions (i.e., the temperature and pressure conditions of the last equilibrium with the mantle source) of primary magmas can be estimated using several well-calibrated geothermometers and barometers (Herzberg and Asimow, 2008; Lee et al., 2009; Putirka, 2008). However, primary magmas are very rarely sampled and their compositions need to be reconstructed from the compositions of the most primitive collected samples. For this, several crucial factors should be considered, such as the forsterite (Fo) content of olivine in equilibrium with mantle, a suitable Fe-Mg exchange reaction coefficient between olivine and melt (K_D) and the oxidation state (oxygen fugacity, fO_2). Among these parameters, the effect of oxidation state on the estimated primary magma compositions of a LIP is generally simplified by assuming $Fe^{2+}/Fe^{total} \sim 0.85$–$0.90$ which is typical for most mantle plume-derived magmas (Ganne and Feng, 2017; Herzberg and Asimow, 2008; Ren et al., 2017; Zhang et al., 2006). However, recent XANES analysis of melt inclusions in host lavas from Canary and Cape Verde Islands showed that mantle plume primary melts can be remarkably more oxidized compared to those of MORB and even subduction zone magmas (Moussallam et al., 2019). If the primary magmas are highly oxidized (Evans et al., 2012; Imai et al., 1993; Kelley and Cottrell, 2009; Moussallam et al., 2019), then the Fe^{2+} content in the magma should be much lower. Because the

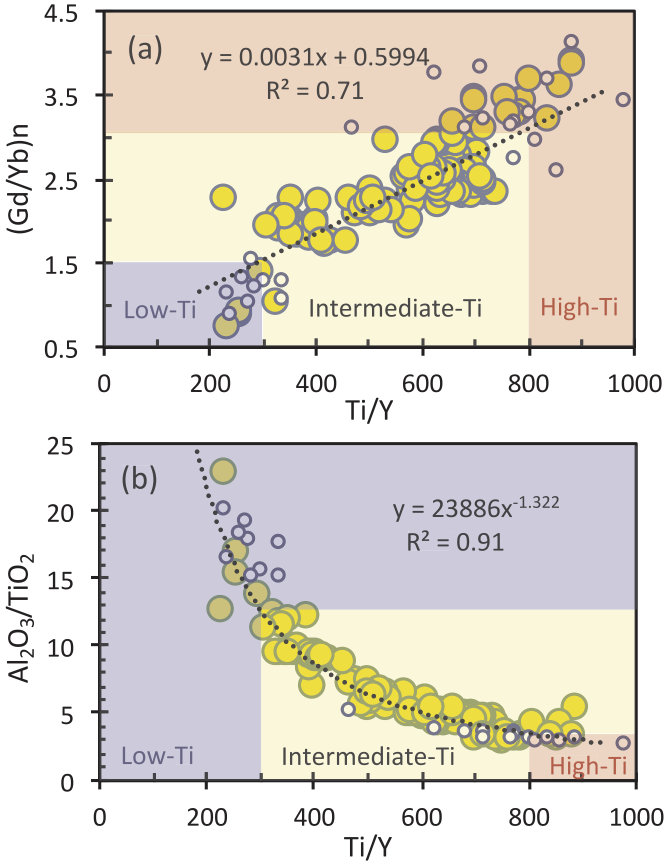

Fig. 2. (a) Ti/Y vs. $(Gd/Yb)_N$ normalized to primitive mantle (Sun and McDonough, 1989) and (b) Ti/Y vs. Al_2O_3/TiO_2 for the ELIP picrites. Large circles are whole-rock data (Chung and Jahn, 1995; Hanski et al., 2010; Kamenetsky et al., 2012; Li et al., 2012; Li et al., 2014; Li et al., 2010; Liu et al., 2017; Song et al., 2001; Tao et al., 2015; Wang et al., 2007; Xiao et al., 2004; Xu et al., 2001; Yu et al., 2017; Zhang et al., 2006) and small circles are melt inclusion data (Kamenetsky et al., 2012). The dotted lines in (a) and (b) show the best linear and power fits calculated on whole rock data and r is the correlation coefficient. The shallow blue, yel low and red fields separates low-Ti, intermediate-Ti and high-Ti samples, respectively. (For interpretation of the references to colour in this figure legend, the reader is referred to the web version of this article.)

exchange reaction between olivine and melt involves Mg^{2+} and Fe^{2+} (Roeder and Emslie, 1970), but not Fe^{3+}, lower Fe^{2+} would propagate to lower MgO in the primary magma and consequently lower melting temperature and mantle potential temperature (Tp) (Herzberg and O'hara, 2002; Putirka, 2005). Knowledge of the fO_2 thus provides insight into the composition and thermal state of primary magmas.

In the southwest China, the intracontinental Emeishan flood basaltic province erupted in the Late Permian (~260 Ma) is a typical mantle plume-related large igneous province (Chung and Jahn, 1995; Shellnutt, 2014; Xu and Liu, 2016; Xu et al., 2001) hosting high-MgO picrites. The main evidences in support of a thermal plume origin are as follows: (1) Thermometry on coexisting olivine and spinel in ultramafic picrites suggests maximum crystallization temperatures of ELIP ~250 °C higher than that of mid-ocean ridge basalts (Xu and Liu, 2016). (2) The eruption that resulted in the emplacement of the ELIP occurred in a brief interval (< 1 Ma) (Zhong et al., 2014). (3) Giant radiating dike swarms, usually interpreted to result from the arrival of a mantle plume at the base of the lithosphere, have been identified in ELIP and coincide with the location of picrites (Li et al., 2015). (4) Relief in ELIP has been interpreted as plume-induced uplift (He et al., 2003; Xu et al., 2004), although this latter hypothesis is debated (Ukstins-Peate and Bryan, 2008). Despite evidences for a thermal plume origin (Shellnutt, 2014 and references therein) and significant progresses made in understanding the genesis of the ELIP picrites (Hanski et al., 2010; He et al., 2010; Kamenetsky et al., 2012; Liu et al., 2017; Ren et al., 2017; Shellnutt and Pham, 2018; Xiao et al., 2004; Xu et al., 2004; Zhang et al., 2019; Zhang et al., 2006), uncertainties remains on the mantle potential temperature (Tp), the nature of the source (lithological makeup), the genesis of the olivine phenocrysts with distinct chemical compositions and the genetic P-T conditions.

The near-primary composition of high-Mg picrites in the ELIP are the best candidates to estimate melting temperature and pressure in the mantle. In addition, olivine phenocrysts with remarkedly different chemical compositions (MORB-type and Hawaii-like, respectively) are excellent candidates to distinguish whether their difference is controlled by lithological heterogeneities or by melting P-T conditions. In this work, we compile compositions of olivine and associated melt inclusions in the high-Mg picrites and demonstrate that the mantle source of the ELIP picrites is dominantly composed of refertilized peridotite, and without requiring the contribution of a pyroxenite component. These results provide additional constraints to restrict the potential range of pressure and temperature melting conditions that can generate the ELIP picrites.

2. Geological background of the ELIP

The Late Permian Emeishan flood basalt province, which is bounded by the Ailao Shan-Red River Fault zone in the west, covers more than 0.3×10^6 km^2 in Yunnan, Guizhou and Sichuan Provinces on the western end of the Yangtze craton (Fig. 1) (Shellnutt, 2014; Xu et al., 2001; Xu et al., 2004). The eruption age (~260 Ma) of the ELIP mostly coincide with the period of Permian-Triassic mass extinction (Xu et al., 2004). Evolved tholeiites are the most commonly occurring mafic-ultramafic volcanic rock in the ELIP, with picrites in a subordinate position (Shellnutt, 2014; Xiao et al., 2004). Associated with these basalts, mafic-ultramafic dikes and layered intrusions are found, with the latter hosting large magmatic oxide and sulfide ore deposits (Shellnutt, 2014). Silicic volcanic and plutonic rocks (mostly syenites and granites) are volumetrically minor (< 5%) but their presence attests of the diversity of magmas produced within the ELIP (Shellnutt, 2014; Zhang et al., 2006). Based on sedimentology and paleogeography, Xu et al. (2004) suggested that three concentric zones of the ELIP can be discriminated, with the crust thickness decreasing from the inner to the outer zone and with high-Mg picrites and mafic-ultramafic intrusions mostly occurring within the inner zone (Chung and Jahn, 1995; Tao et al., 2015; Zhang et al., 2006).

3. Geochemical data

3.1. Whole rock

We compiled geochemical data on the ELIP picrites from several previous studies (Chung and Jahn, 1995; Hanski et al., 2010; Kamenetsky et al., 2012; Li et al., 2012; Li et al., 2014; Li et al., 2010; Liu et al., 2017; Song et al., 2001; Tao et al., 2015; Wang et al., 2007; Wu et al., 2018; Xiao et al., 2004; Xu et al., 2001; Yang and Liu, 2019; Yao et al., 2019; Yu et al., 2017; Zhang et al., 2019; Zhang et al., 2006). Here we only summarize key observations used in the subsequent discussion. Because samples with MgO < 10 wt% could have suffered from clinopyroxene fractionation (Hanski et al., 2010; Ren et al., 2017), they are not included in the following discussion. Based on the TiO_2 contents and Ti/Y ratios, a low-Ti end-member (Ti/Y < 300) and a high-Ti end-member (Ti/Y > 800) can be recognized (Kamenetsky et al., 2012; Ren et al., 2017). Most of the ELIP picrites have Ti/Y ratios between the two end-members, forming a continuous compositional spectrum (Kamenetsky et al., 2012). There is a positive correlation between Ti/Y and $(Gd/Yb)_N$ ratios and a negative correlation between Ti/Y and Al_2O_3/TiO_2 ratios (Fig. 2). Except for three samples, most picrites have

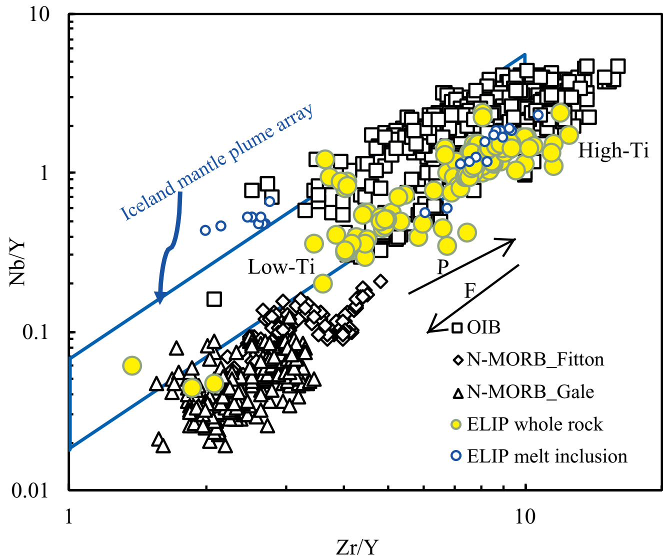

Fig. 3. Whole rock Nb/Y vs. Zr/Y for the ELIP picrites. Data source: OIB (Fitton et al., 2003), N-MORB (Fitton et al., 1997; Gale et al., 2013) and field of Iceland mantle plume array (Fitton et al., 1997). F and P arrows indicate the approximate effects of increasing degree and pressure of melting, respectively.

higher Nb/Y and Zr/Y ratios than those of MORB, and close to the ratios in OIB, inside the Iceland mantle plume array defined by Fitton et al. (1997) (Fig. 3).

3.2. Olivine

We compiled 2256 olivine compositions from ELIP with Fo (Forsterite) contents ranging from 75.9 to 93.5 (Hanski et al., 2010; Kamenetsky et al., 2012; Liu et al., 2017; Putirka et al., 2018; Ren et al., 2017; Yang and Liu, 2019; Yao et al., 2019; Yu et al., 2017; Zhang et al., 2019). We observe a positive correlation between NiO and Fo contents and a negative correlation between MnO and Fo contents (Fig. 4). At a given Fo, olivines in low-Ti picrites have systematically higher Mn and lower Ni contents than high-Ti samples (Fig. 4). Additional olivine trace element data show Ca contents between 1500 and 4000 ppm (Fig. 4c), Mn/Zn ratios of 12–22 and 10^4*Zn/Fe values of 7–14 (Fig. 5).

3.3. Melt inclusions

The compositions of olivine-hosted melt inclusions were compiled from Hanski et al. (2010), Kamenetsky et al. (2012) and Ren et al. (2017). MgO content varies from 4.4 to 21.6 wt%, CaO content from 8.3 to 19.3 wt% (Fig. 6a) and Na_2O + K_2O from 0.8 to 4.4 wt% (Fig. 6b). The FC3MS values (Yang et al., 2016) range from −0.4 to 0.6 (Fig. 6b and c). Melt inclusions from the Dali picrites have compositional variations covering the all compositional spectrum from low to high-Ti picrites, albeit their whole rock is confined to intermediate-Ti compositions (Ren et al., 2017).

4. Discussion

4.1. A refertilized peridotite mantle source for the ELIP picrites

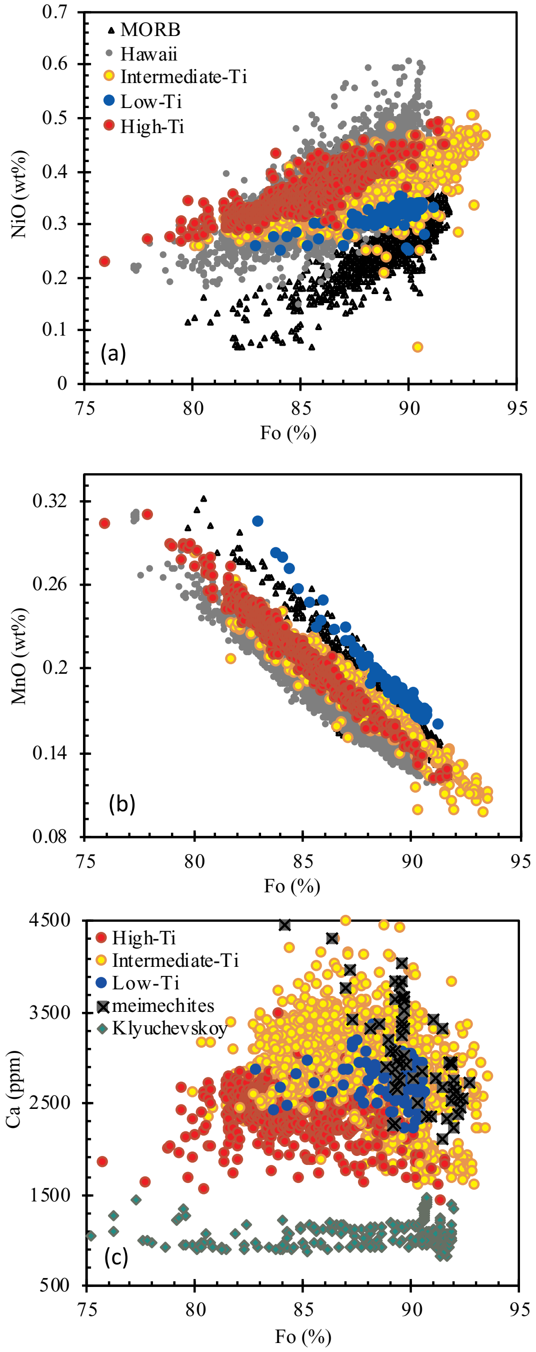

Fig. 4. Olivine Fo content vs. (a) NiO content, (b) MnO content and (c) CaO content for the ELIP picrites (Hanski et al., 2010; Kamenetsky et al., 2012; Liu et al., 2017; Putirka et al., 2018; Ren et al., 2017; Yu et al., 2017). In (a) and (b), data source for MORB and Hawaii are from Sobolev et al. (2007). In (c), data source for Klyuchevskoy arc magmas and Siberian meimechites are from Gavrilenko et al. (2016) and Sobolev et al. (2009), respectively.

Previous studies suggested peridotite- and pyroxenite-dominated sources for the low-Ti and high-Ti ELIP picrites, respectively (He et al., 2010; Kamenetsky et al., 2012; Liu et al., 2017; Yu et al., 2017; Zhu et al., 2018). These conclusions were mostly based on the observation that olivine Ni and Mn contents in the low-Ti and high-Ti ELIP samples fall in the fields of MORB and Hawaii olivines, respectively (Fig. 4). In fact, Sobolev et al. (2007) suggested that a pyroxenite source can be identified from olivine phenocrysts having high Ni and high Fe/Mn compositions. Based on the relatively constant Pb isotope ratios of the melt inclusion, Ren et al. (2017) suggested that both low and high-Ti picrites are formed by a single pyroxenitic mantle source and explained the wide range of Ti contents with picrites sampling different depths of the melting column. However, Xu and Liu (2016) found a roughly positive corelation between olivine Ni content and olivine-spinel Al temperature, suggesting olivine compositions may be controlled by temperatures of melting and/or crystallization. In fact, recent experimental work (Matzen et al., 2013; Matzen et al., 2017b) showed that partition

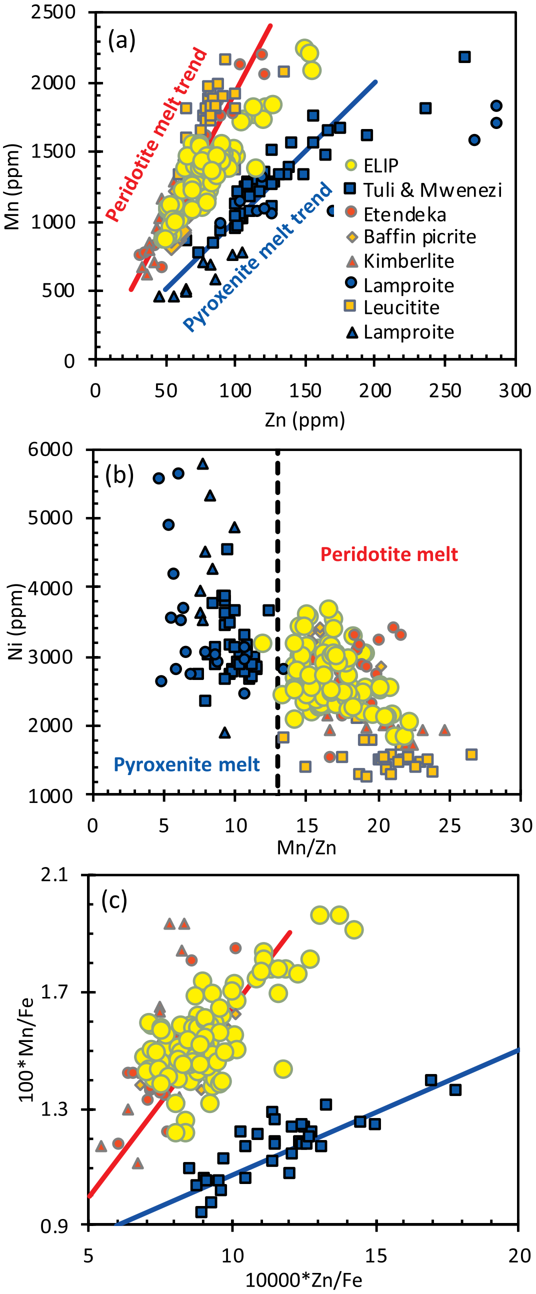

Fig. 5. Trace element data of olivines from the ELIP picrites. (a) Zn vs. Mn, (b) Ni vs. Mn/Zn and (c) 100*Mn/Fe vs. 10,000*Zn/Fe. Shown for comparison are data of Etendeka, Tuli and Mwenezi flood basalts in South Africa, picrites of Baffin, group 1 kimberlite and lamproite (see Howarth and Harris, 2017 and references therein). In (a) and (c), the red line represents peridotite melt trend and the blue line is pyroxenite melt trend, respectively (Howarth and Harris, 2017). In (b), the vertical dashed line can be used to discriminate pyroxenite melt from peridotite melt (Howarth and Harris, 2017). (For interpretation of the references to colour in this figure legend, the reader is referred to the web version of this article.)

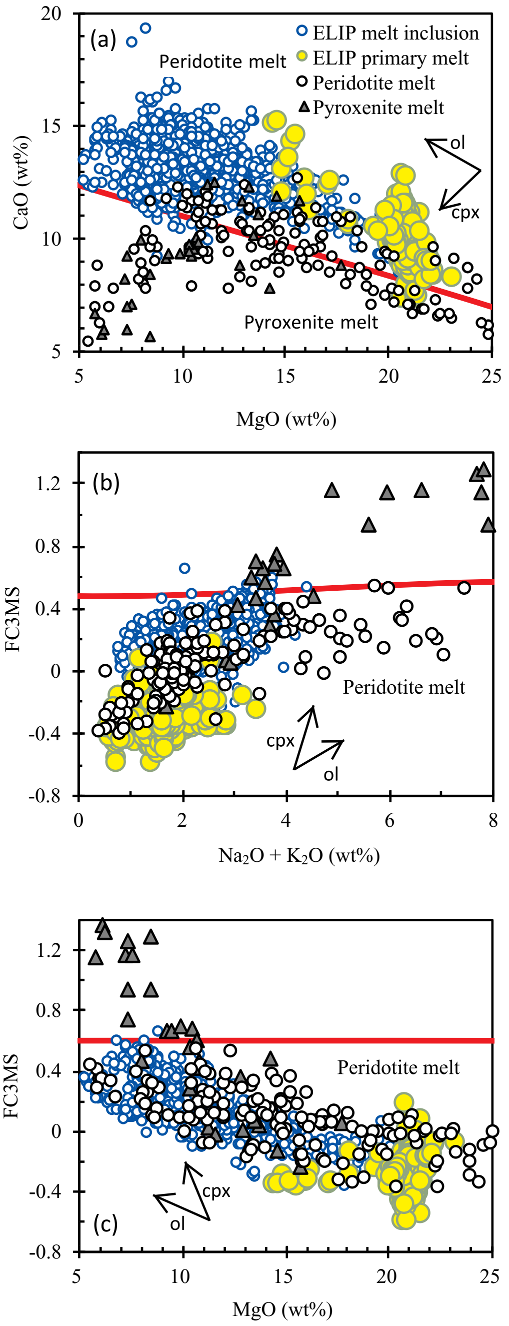

Fig. 6. (a) CaO vs. MgO, (b) FC3MS (FeO/CaO-3*MgO/SiO_2, wt%) vs. Na_2O + K_2O and (c) FC3MS vs. MgO of melt inclusions and their primary magmas for the ELIP picrites. Data for experimental pyroxenite melt and peridotite melt are compiled by Yang et al. (2016). In (a), the red line discriminates pyroxenite melt and peridotite melt (Herzberg and Asimow, 2008); in (b) and (c), the red lines indicate the upper boundary for peridotite melts (Yang et al., 2016). Fractionation vectors for olivine (ol) and clinopyroxene (cpx) are also indicated. (For interpretation of the references to colour in this figure legend, the reader is referred to the web version of this article.)

coefficient for Ni and Mn can be significantly affected by melting conditions such as pressure and temperature. Hence, it is necessary to re-investigate the potential role of pyroxenite in the genesis of ELIP picrites by combining olivine compositions with other chemical tracers of the nature of the source, although Yao et al. (2019) proposed that olivine compositions in some ELIP picrites can be derived from a peridotite source.

The CaO content in the magma at a given MgO content was initially proposed as a way to discriminate peridotite- and pyroxenite-derived magmas (Herzberg and Asimow, 2008). Both melt inclusion and primary magma compositions plot in the field of peridotite melts (Fig. 6a). High Ca contents observed in olivine (Fig. 4c) also favors a peridotite source (Herzberg, 2011). However, mantle pyroxenites cover a large compositional range (Lambart et al., 2013) and the discriminant line proposed by Herzberg and Asimow (2008) cannot be generalized to all pyroxenites; melt derived from Ca-rich pyroxenites will plot above the discriminant line (Herzberg, 2011; Lambart et al., 2013) and will crystallize olivine with high Ca content. Furthermore, many peridotite melts from Yang et al. (2016) plot below the lower limit of peridotite melts of Herzberg and Asimow (2008). This indicates that certain peridotite melts can also be featured by low CaO content, thus the discriminant line of CaO-MgO cannot be used alone to distinguish between pyroxenite melts and peridotite melts. Using a statistical analysis of a large amount of partial melting experiments, Yang and Zhou (2013) and Yang et al. (2016) proposed that the FC3MS (FeO/CaO-3*MgO/SiO_2, in wt%) parameter can help with distinguishing between pyroxenite- and peridotite-derived melts. Their analysis demonstrates that the upper boundary of the FC3MS value for peridotite melts is 0.65, while melts derived from pyroxenites cover a much larger range (−0.9 to 1.7). Both the melt inclusion and the calculated primary magma compositions of the ELIP picrites present low FC3MS values, consistent with partial melting of a peridotite source (Fig. 6b and c). However, we highlight that, once again, such low FC3MS values can also be produced by pyroxenite melting (e.g., CaO-rich pyroxenite will also generate low FC3MS values) and consequently cannot be used alone to eliminate a potential pyroxenitic source.

Finally, Howarth and Harris (2017) recommended the use of FTRE (first-row transition elements) to discriminate between pyroxenite and peridotite melts. Howarth and Harris (2017) showed that most olivines from continental flood basalt presenting a potential pyroxenite signature (i.e., high Ni, low Mn for a given Fo content) also have Mn/Zn < 13. The Zn vs. Mn (Fig. 5a), Ni vs. Mn/Zn (> 13, except for one sample with a value of 12) (Fig. 5b) and 100*Mn/Fe vs. 10,000*Zn/Fe (Fig. 5c) trends for ELIP olivines are very similar to those from Etendeka flood basalts in South Africa (Howarth and Harris, 2017), picrites of Baffin (De Hoog et al., 2010) and leucitite and group 1 kimberlite (Ammannati et al., 2016), all of which were interpreted to derived from a peridotite mantle source (Howarth and Harris, 2017 and references therein). At 1.5–2 GPa, peridotites produce melt with 10000*Zn/Fe ≤12 while eclogitic melt can extend toward higher values (Le Roux et al., 2011). At 3 GPa, ratios in peridotite melts can reach values up to 13 (Davis et al., 2013). All but three ELIP samples have values ≤13 and we cannot exclude that peridotite could produce melt with even higher ratios at higher pressures. Therefore, the presence of pyroxenites in the mantle source is not necessary to explain the melt inclusion compositions and the olivine data from the ELIP picrites. Hence, we favor a source lithology dominated by mantle peridotite under the ELIP. Finally, in the plot of Nb/Y vs. Zr/Y, the ELIP picrites compositions are close to mantle plume-influenced Iceland basalts (Fitton et al., 1997) and OIB (Fitton et al., 2003), and different from compositions of N-MORB (Fitton et al., 1997; Gale et al., 2013) (Fig. 3). This suggests that the source of ELIP picrites contains an enriched component, consistent with a refertilized mantle peridotite. This is supported by isotopic analyses on Emeishan basalts that support the presence of several mantle components in the source (Chung and Jahn, 1995; Fan et al., 2008; Shellnutt, 2014; Xiao et al., 2004).

4.2. *Primary magma compositions*

To estimate the P-T conditions of melt segregation from the mantle, we calculate the primitive magma compositions using Lee et al. (2009)’s spreadsheet by correcting for olivine accumulation/fractionation in the picrites and for olivine fractionation in melt inclusions. For the Fe-Mg exchange reaction coefficient between olivine and melt (K_D), we use a constant $K_D = 0.34$ to reflect the high MgO content of the primitive magma and the high pressure of crystallization (most of them crystallized at pressures over 1 GPa) (Herzberg and O'hara, 2002; Matzen et al., 2011; Putirka, 2005; Tao et al., 2015), and the maximal Fo content observed in the ELIP (Fo = 93.5%) (Hanski et al., 2010; Kamenetsky et al., 2012; Liu et al., 2017). Choices for water content and oxygen fugacity of the primary magmas are described below.

Parman et al. (2011) demonstrated that the maximum Al_2O_3 concentration in the melt reached along a liquid line of descent (LLD) correlates well with dissolved H_2O concentration. Hence, by identifying the maximum Al_2O_3 in related natural samples we can estimate of the pre-eruption H_2O concentrations (Al_2O_3-LLD). Wang et al. (2016) used the Al_2O_3-LLD method to estimate the pre-eruptive melt H_2O concentrations for various continental flood basalt provinces. Additionally, they showed that continental flood basalts display enrichment of fluid-mobile elements and depletion of high-field-strength elements, similar to those evolved in the subduction environment and used the correlation between H_2O/Ce and Ba/La, Ba/Nb and Rb/Nb observed in arc magmas to estimate the H_2O/Ce ratio in primary melts of continental flood basalts. Finally, they calculated the primary Ce concentration (in equilibrium for Fo_{91}) to estimate the primary melt H_2O content. With this approach, primary melts from Emeishan continental flood basalt show high H_2O concentration of 4–5.6 wt%.

Using water content measured in clinopyroxene phenocrysts (Wade et al., 2008), and after correction for previous crystallization of olivine, Liu et al. (2017) obtained slightly lower water content (~3.4 wt%) in ELIP primary magmas. It is worth noting that these two approaches are indirect methods. Wang et al.'s (2016) approach depends on the assumption that correlations between H_2O and Al_2O_3 and with H_2O/Ce are the same in arc magmas and continental flood basalts and, Liu et al. (2017) assumed that the water content in clinopyroxene has a mantle origin. Nonetheless, these results, obtained with two independent method, support a wet primary magma composition, comparable to contents reported in melt inclusions from arc magmas (e.g., Kelley and Cottrell, 2009).

A third indirect method is to estimate the water content of the primary magmas using the calcium content in olivine (Gavrilenko et al., 2016). In fact, the presence of water in the primary magma tends to decrease the partitioning coefficient of calcium between olivine and melt and results in lower Ca content in magmatic olivine (Feig et al., 2006). Fig. 4c shows that the Ca contents in island arc olivines from Klyuchevskoy volcano are around 1000 ppm, while in ELIP olivines, supposed to have crystallized from magmas with similar water content (Mironov and Portnyagin, 2011), the Ca content varies between 2000 and 4000 ppm, suggesting that ELIP olivines are derived from a volatile-deficient source. Primary magmas calculated for ELIP picrites contain up to 23 wt% MgO (see below). On the contrary, MgO content from primitive melt inclusion from the Klyuchevskoy arc magmas are up to 12 wt% (Mironov and Portnyagin, 2011). Using Gavrilenko et al.'s model (2016), an increase from 12 to 23 wt% MgO and a decrease from 4 to 0 wt% H_2O in the melt would result into a maximal increase in Ca content of 1000 ppm (see Fig. 7 in Gavrilenko et al., 2016) and would not explain the range of Ca content observed in the ELIP olivines. Additionally, Gavrilenko et al. (2016) noted that their model fails to explain the partitioning of CaO for meimechites olivines. Meimechites are alkali- and MgO-rich melts likely formed at high pressure (Fig. 4c; Sobolev et al., 2009). Interestingly, melt inclusions in meimechites olivines also contain high water content up to ~3.88 wt% (Ivanov et al., 2018). The detailed reason of this discrepancy is beyond the scope of this paper, but this suggests that other parameters must control the Ca content in olivine. MgO should not be the sole adjustable parameter to describe the partitioning of CaO between olivine and melt. Therefore, we cannot directly compare the Ca content in olivine from various geodynamics setting to decipher the water content in the magma; the water effect on Ca partitioning requires further evaluation.

In the following discussion, we focus on the wet end-member, supported by two of the three methods described above, and use a mean water content of 3.4 wt% (Liu et al., 2017). However, because this parameter might strongly affect the pressure and temperature estimate, its impacts on our conclusions are discussed in details later (see Section 5).

Similar to the water content, the choice of the oxygen fugacity is likely to affect the pressure-temperature estimates. Under-estimating the fO_2 results in overestimating the melting temperature. Using the

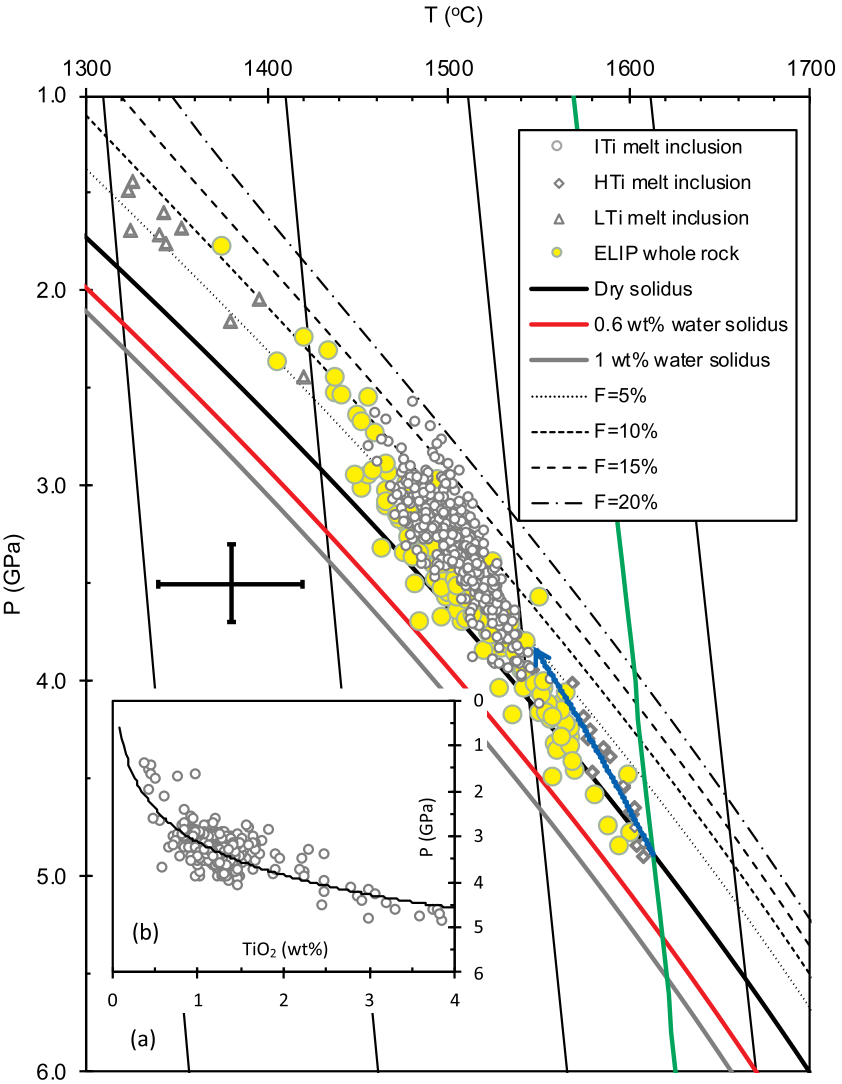

Fig. 7. (a) Melting P-T conditions underneath the ELIP. The equilibrium P-T are calculated using the peridotite-melt model of Lee et al. (2009). The anhydrous solidus is from Hirschmann (2000). Red and grey lines are calculated solidus according to the model of Katz et al. (2003) for hydrous peridotite with 0.6 wt% and 1.0 wt% H_2O, respectively. Near-vertical lines are mantle adiabats with Tp of 1300, 1400, 1500 and 1600 °C (black) and 1560 °C (green), respectively. Melt fraction lines with F = 5, 10, 15 and 20% are calculated using the model of Kelley et al. (2010) for source with water content of 0.6 wt% (Liu et al., 2017) and partition coefficient for water between mantle and melt of 0.012 (Kelley et al., 2006). The curved blue line represents the possible melting adiabat, which is roughly fitted by the array of P-T data of ELIP picrites. This array intersects the anhydrous peridotite solidus at ~5 GPa, giving a minimal Tp of ~1560 °C. (b) Insert shows TiO_2 contents of melt inclusions vs. melting pressure for the ELIP picrites. (For interpretation of the references to colour in this figure legend, the reader is referred to the web version of this article.)

composition of the coexisting olivine and spinel from Eimeshan picrites, Bai et al. (2019) calculated a large range of oxygen fugacities for the parental magmas with values as high as FMQ + 2.5. They interpreted these elevated fO_2 as inherited from an oxidized mantle source (Evans et al., 2012). This result, comparable with the most recent XANES results for melt inclusion in mantle plumes primary melts (Moussallam et al., 2019), is also supported by the high water contents (excellent candidate as oxidation agent) estimated in ELIP primary magmas. The arc-like oxidized and hydrous features of the ELIP picrites may also be critical factors for early saturation of Fe-Ti oxides (Bai et al., 2019) and the formation of colossal magmatic Cu-Ni-PGE sulfide ore deposits present in the Emeishan large igneous province (e.g., Ballard et al., 2002; Sun et al., 2013). It is likely, however, that the fO_2 varies in the mantle source (i.e, Bai et al.'s (2019) estimates vary from FMQ to FMQ + 2.5). In the following discussion, we focus on the oxidized end-member, but, in parallel with our tests on the impact of the water content, the impact of the fO_2 is discussed in section 5.

Hence, prior to each incremental step of olivine addition or subtraction, the magma ferric/ferrous iron ratio was calculate using the model of Kress and Carmichael (1991) with a fO_2 value of FMQ + 2.5 for the ELIP primitive magmas. The corresponding $Fe^{3+}/\Sigma Fe$ ratios range from 0.27 to 0.34, with an average value of 0.30 ± 0.01 (1σ), which is similar to those of mantle plumes primary magmas (0.27–0.30) reported by Moussallam et al. (2019). This is significantly higher than the values used in previous estimations (e.g., 0.1 in Hanski et al. (2010) and Ren et al. (2017) and 0.15 in Zhang et al. (2006)). The primary melts of whole rock samples and melt inclusions have MgO content of ~17.2–23.9 wt% and 14.0–23.2 wt%, respectively. It is worth noting that although Ren et al. (2017)'s results were based on the assumption that $K_D = 0.30$ and $Fe^{3+}/\Sigma Fe = 0.1$, we obtain similar primary magmas compositions.

4.3. Mantle melting conditions

The depth and temperature at which the ELIP primary magma is in last equilibrium with the peridotite mantle source can be calculated using the olivine-liquid Fe-Mg exchange thermometer model and the liquid SiO_2 activity barometer model of Lee et al. (2009). Using the water content estimated by Liu et al., 2017 (3.44 ± 0.89 wt%) and the calculated primary magma compositions, we show that the pressure and temperature conditions of last equilibrium with the mantle calculated on the whole rock sample (1.8–4.8 GPa and 1378–1598 °C) overlap with the conditions calculated with melt inclusions (1.5–4.9 GPa and 1323–1608 °C; Fig. 7). Whole rocks, however, cover a slightly smaller range of conditions (Fig. 7), highlighting a smaller compositional variability of the lavas, consistent with modest magma mixing before eruption of the picrites (Kamenetsky et al., 2012).

Calculations also reveal a negative correlation between the TiO_2 contents of the melt inclusion and the segregation pressures (Fig. 7b): the high-Ti melt inclusions are segregated at significantly higher P-T conditions (T = 3.9–4.9 GP and 1550–1610 °C) than the low-Ti melt inclusions (1.5–2.4 GPa and 1320–1420 °C) (Fig. 7a). We estimate the melting degree from the melting conditions using the hydrous melting model of Kelley et al. (2010), an initial H_2O content in the mantle source of 0.6 wt% (Liu et al., 2017) and a partition coefficient for water between mantle and melt of 0.012 (Kelley et al., 2006). The degree of melting broadly increases with decreasing pressure, from ~0 to 10–15% in whole rock, consistently with the incompatible behavior of Ti during partial melting of peridotite. A small percentage (~3%) of the intermediate-Ti melt inclusions, however, record higher melt fractions higher than 15%. This might be the result of a sample bias. In fact, plumes are usually assumed to present a temperature gradient from the center to the rim (e.g., Sobolev et al., 2005). We have significantly more data on intermediate compositions than on low- and high-Ti compositions; variations observed in intermediate-Ti melt inclusions could reflect a larger recorded range of temperatures. Alternatively, clinopyroxene fractionation may play a role in this apparent discrepancy. In fact, ELIP picrites crystallized at high pressure (> 1GPa) and experimental results from Villiger et al. (2004) showed that cpx crystallization at 1 GPa can start as early as the melt reached 12 wt% MgO. In these calculations however, we used Lee et al.'s model (2009) that only takes into account olivine fractionation. The ~3% of melt inclusions that show melt fractions higher than 15% all have MgO contents between 10 wt% and 12 wt%. Inaccurate fractionation correction can significantly overestimate temperatures and depths of melting (Till et al., 2012). The array of P-T data for the ELIP intersects the anhydrous peridotite solidus at ~5 GPa (Fig. 7a), corresponding to a mantle potential temperature of ~1560 °C (Lee et al., 2009). Because the mantle source is hydrous, the intersection of the ELIP magma with the wet solidus is likely to be at much higher pressure. Hence, this temperature should be considered as a minimum value. Extrapolating the trend produced by the data down to the intersection with the 0.6 wt% water solidus suggest a pressure of 5.4 to 6 GPa that would correspond to a potential temperature close to 1600 °C. However, magmatic productivity of hydrous peridotite at low melting degree (Asimow and Langmuir, 2003; Katz et al., 2003) is low and melting below the dry solidus is unlikely to significantly affect the decompression path. This mantle potential temperature is remarkably (> 210 °C) higher than that (~1350 °C) of the ambient MORB mantle (Herzberg et al., 2007), and is consistent with the crystallization temperature difference (~250 °C) obtained from the Al-in-olivine thermometry (Xu and Liu, 2016).

4.4. *Pressure-dependent compositional variation of olivines*

When primary magmas ascend adiabatically, the decrease in temperature can result in an increase in partition coefficient of Ni between olivine and melt (i.e., the "ΔT effect"). For instance, according to the experimental calibration of Matzen et al. (2017a), primary melts of mantle peridotite from ~100 km depth and in equilibrium with residual olivines with 2800–3100 ppm Ni (~0.36% NiO; Herzberg et al., 2013) at ~1550 °C, will crystallize olivine near the surface at ~1400 °C with 3700–3900 ppm Ni (~0.48% NiO), similar to ELIP olivine nickel contents. Therefore, T-P conditions of peridotite melting can be significant.

To test if variation of magma segregation pressures is consistent with the compositional variability of the ELIP olivines, we compare the olivine MnO_{89} and NiO_{89} (i.e., the MnO and NiO contents in olivines corrected to Fo_{89} along a crystal line of descent) with the compositions of experimental and natural olivines reported by Matzen et al. (2017b). Both data sets display negative correlations (Fig. 8). Olivine from high-Ti samples have NiO_{89} higher and MnO_{89} lower than those in low-Ti samples (Fig. 8). The high-Ti olivine present similar NiO_{89} to olivine from experiments performed at 3–4.5 GPa (Fig. 8) and NiO and MnO contents comparable to contents observed in Hawaiian olivine (Fig. 4). The low-Ti olivines present similar NiO_{89} to olivine from experiments performed at 1 GPa and NiO and MnO contents intermediate between those observed in MORB and in Hawaiian olivine (Fig. 4). These observations are consistent with the pressure range calculated in Fig. 7 (~ 1.5–4.5 GPa) and with the correlation between Ti content in melt inclusions and pressure of segregation (Fig. 7b), supporting our conclusions that both high-Ti and low-Ti olivine compositions can be explained by melting a peridotite source. We note, however, that the NiO_{89}-MnO_{89} correlation described by the ELIP olivines presents a gentler slope than the correlation described by experimental and natural olivines (Fig. 8). This discrepancy could be produced if primary melts were derived from mantle peridotites that are heterogeneous with respect to Ni and Mn contents. Alternatively, this discrepancy could also reflect the effects of both the high oxygen fugacity and the presence of water in the mantle source. In fact, Mysen and Dubinsky (2004) showed that (1) the increase of the oxygen fugacity is accompanied with a decrease of the degree of polarization of the melt (NBO/T) and (2) the ${K_{DMn}}^{olivine/melt}$ increases with decreasing NBO/T. Hence, the increase of the oxygen fugacity in the mantle could result in higher MnO contents in the magmatic olivines (consistent with the high MnO_{89} of the low-Ti olivines compared to 1 GPa experimental olivines and natural MORB olivines; Fig. 8). Moreover, under hydrous conditions, Mn becomes strongly compatible in garnet, but the presence of water does not significantly affect the Mn partitioning behavior in olivine and pyroxene (Balta et al., 2011). Hence, in the presence of garnet, at pressures relevant for high-Ti olivines, magmas generated under hydrous conditions have lower Mn content than magmas generated under anhydrous conditions (explaining the gentler slope for the ELIP olivine observed in Fig. 8). The detailed investigation of the combined effects of water and oxygen fugacity is, however, beyond the scope of this work and is worthy of future experimental investigation.

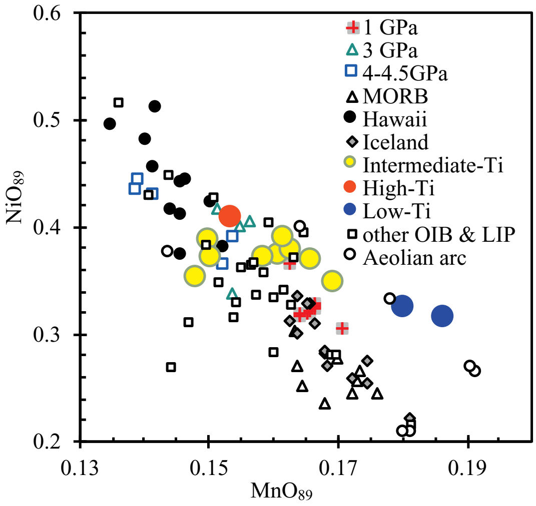

Fig. 8. Olivine NiO_{89} vs. MnO_{89} for the ELIP picrites (Kamenetsky et al., 2012; Liu et al., 2017; Yu et al., 2017). The MnO and NiO contents in olivines were corrected to Fo_{89} along a fitted crystal line of descent following the method of Matzen et al. (2017b). Compositions of natural (MORB, Hawaii, Iceland and other OIB & LIP) and model (1, 3 and 4–4.5 GPa) olivines crystallized from peridotite primary melts are from Matzen et al. (2017b). Data for Aeolian arc are from Zamboni et al. (2017).

4.5. *Geodynamic scenario for generation of the ELIP low-Ti and high-Ti picrites*

The shallowest depth of melt segregation is approximately 50 km (Fig. 7a), which is inside the present-day lithospheric mantle (Jiang et al., 2018; Xu et al., 2004). Hence, there are two possible scenarios for the genesis of the ELIP picrites: (1) conductive reheating of the subcontinental lithospheric mantle (SCLM) above the solidus of mantle peridotite during impingement of the mantle plume, or (2) enhanced decompression melting within the upwelling mantle plume during thermal erosion-related lithospheric thinning.

If the magmas were last in thermal equilibrium with the SCLM beneath the depth of Moho, then the calculated pressures would imply that the ELIP magmas were either melting products derived from the lithospheric mantle, or they were mantle plume melts re-equilibrated with the SCLM during melt transported upward through the lithospheric mantle, at depths ranging from ~50 to ~150 km (Fig. 7a). Considering the high magmatic H_2O content (Liu et al., 2017) and oxygen fugacity of the primary magmas, we can reasonably infer that the potential SCLM source could have been previously metasomatized by ancient subduction events. Because the western margin of the Yangzte Craton was an active continental arc during the late Proterozoic time (Song et al., 2001; Xiao et al., 2004), SCLM underneath the ELIP could have been metasomatized and refertilized by melts/fluids derived from subducted slabs. However, there are some flaws in this model, indicating that the SCLM may not act as the appropriate source. Firstly, Liu et al. (2017) suggested that high H_2O/Ce ratios (~1800) of the ELIP picrites compared to that of the SCLM-derived melt (H_2O/Ce $<$ 700) can exclude the SCLM as the mantle source. In addition, the Re-Os isotopic analyses on the ELIP picrites show no evidence for a massive contribution of metasomatized SCLM in their mantle source (Zhang et al. (2008). Furthermore, an ancient metasomatized SCLM usually displays highly heterogeneous and enriched Sr-Nd-Pb isotopic signatures (Gao et al., 2008; Turner and Hawkesworth, 1995; Xiao et al., 2004). On the contrary, whole rock (Sr-Nd) and melt-inclusion (Pb) isotopic ratios are relatively constant (Kamenetsky et al., 2012; Ren et al., 2017), suggesting various degree melting of a relatively homogeneous mantle source.

Although the above arguments cannot fully reject the potential contribution from the assimilation of the SCLM during melt transport, we favor an alternative geodynamic scenario for the origin of the ELIP magmas: the decompression melting during upwelling of a hot hydrous mantle plume, accompanying by catastrophic lithospheric thinning (Xu et al., 2001). The unusually high water content and oxygen fugacity may be related to a hydrous reservoir in the deep mantle, either in the mantle transition zone (MTZ) captured by plume during upwelling, or in the geophysically observed large low-shear-velocity provinces (LLSVPs) where the ELIP plume might originate (Liu et al., 2017; Wang et al., 2016). During mantle plume emplacement, low degree melting at greater depths yields high-Ti primary melts, while high degree decompression melting at lower depths produces low-Ti magmas (Fig. 7b) (Xu et al., 2001). The high-Ti magmas would separate from the mantle source at high pressure, ascend adiabatically to shallower depths, then precipitate primitive olivines with higher Ni and lower Mn contents than olivines crystallized from low-Ti magmas derived from shallow depth. This model is supported by variation of the primitive mantle normalized rare earth element ratios, such as $(Gd/Yb)_N$. The low-Ti magmas display low $(Gd/Yb)_N$ ratios ($<$ 1.5) (Fig. 2a), which suggest that they were derived from mainly a spinel peridotite source, at a depth shallower than 70 km (Xu et al., 2001). In contrast, the high-Ti samples have relatively high $(Gd/Yb)_N$ ratios ($>$ 2.5) (Fig. 2a), favoring an origin in the garnet stability field (Xu et al., 2001).

5. Potential uncertainties

The absolute P-T estimates rest strongly on our assumptions of water content and $Fe^{3+}/\Sigma Fe$ ratio of the primary magmas. Except for the water content of Dali picrites (Liu et al., 2017), no other analyses have been reported so far. However, the H_2O content of the ELIP primary melts in other areas may be different from the Dali picrites, and could be variable from one location to another. Furthermore, available water data in the ELIP picrites is calculated on the basis of clinopyroxene-melt equilibrium. Considering that olivine or spinel usually precipitates as a liquidus phase earlier than clinopyroxene, the published water content based on clinopyroxene-melt equilibrium may thus only be regarded as a maximum value. We want to highlight, however, that the high pressure of crystallization of the ELIP picrites ($>$ 1GPa) enhances the stability of clinopyroxene and this later is likely to start to crystallize early in the crystallization sequence (Husen et al., 2016; Villiger, 2004; Villiger et al., 2007). Likewise, the $Fe^{3+}/\Sigma Fe$ ratios of the ELIP primary magmas are also not well constrained. There is no direct measurements (e.g., XANES) of olivine-hosted melt inclusions in ELIP picrites; Bai et al.'s results (2019) are indirect measurements from olivine and spinel compositions (Ballhaus et al., 1991). Furthermore, oxygen fugacity of the erupted picrites may not simply reflect the oxidation state of the primary magma at depth. In fact, when primary magmas segregate from its source and ascend adiabatically, they might oxidize during decompression. The consequence is that the oxygen fugacity of primary magmas at mantle depth can be 1–2 log units lower than those at the surface (Kress and Carmichael, 1991).

Given above potential uncertainties in water content and oxygen fugacity and to better understand how these variations will propagate to estimation of P-T, we did a series of calculations using different water contents and $Fe^{3+}/\Sigma Fe$ ratios as input. The summary of the effects of primary melt water H_2O content and $Fe^{3+}/\Sigma Fe$ on the estimated segregation P-T conditions for primary magmas of melt inclusions is presented in Fig. 9. Individual calculations are plotted in the Supplementary Figures. Decreasing the water content and the oxidizing conditions both result into increasing the average pressure and widening the range of pressures at which magma segregation occurs. The average pressure of segregation for the wet and oxidized end-member is 3.3 GPa and magma segregation occurs between 1.4 and 4.9 GPa. For comparison, using primary magmas with 1 wt% H_2O and $Fe^{3+}/\Sigma Fe$ = 0.1, the average pressure is 6.6 GPa and the pressure of segregation varies from 2.4 to 10.5 GPa. Hence, calculations under drier and less oxidized conditions shift the estimation to higher P-T conditions, and our calculations provide a minimum segregation P-T for the ELIP picrites and consequently a minimum estimation of the potential temperature. One additional scenario would be to consider variations of the water content and oxygen fugacity in the mantle source. In fact, Bai et al. (2019) showed that low-Ti picrites can record a significantly lower fO_2 (= FQM) than high-Ti picrites. To test this hypothesis, we used the extreme scenario where high-Ti picrites would be formed by a wet and oxidized mantle (3.4 wt% H_2O and $Fe^{3+}/\Sigma Fe$ = 0.3), while low-Ti picrites

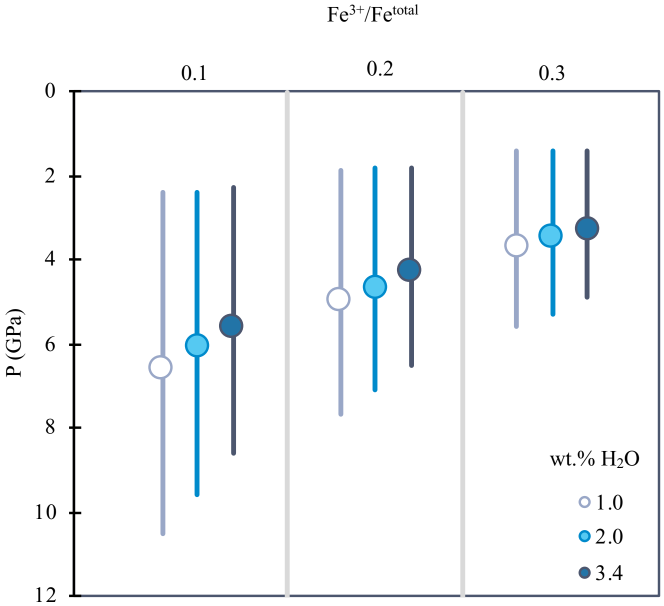

Fig. 9. Averages (circles) and ranges (vertical bars) of pressures of melt segregation for primary magmas calculated from melt inclusions using Lee et al. (2009)'s model as a function of the $Fe^{3+}/\Sigma Fe$ ratio and for 1, 2 and 3.4 wt% H_2O.

would be produced by a mantle with 1 wt% H_2O at $Fe^{3+}/\Sigma Fe = 0.1$. In this case, the average pressure of Hi-Ti picrites is 4.5 GPa and the average pressure of low-Ti picrites is 3.2 GPa. So, even in this extreme scenario, a difference of segregation pressure between high- and low-Ti picrites over 1 GPa is required to explain the genesis of the ELIP picrites. Hence, the assumption whether melting of a peridotite mantle source at different P-T conditions can explain the differences between high-Ti and low-Ti picrites is robust and our simple modelling places a first-order constrain on genesis of the ELIP picrites.

6. Conclusions and future directions

Olivine, melt inclusion and whole-rock geochemical data on picrites from the Emeishan large igneous province support a scenario where no pyroxenite component is involved, but in which picrites are crystallizing from magmas segregated at different depths along an adiabatic path controlled by the decompression melting of a relatively homogeneous hydrous peridotitic mantle plume source. The peridotite source could have been refertilized by fluid/melt from recycled oceanic crust. We also highlight that, while several pieces of evidence suggest that the mantle source of the Emeishan picrites is hydrous and oxidized, further work, such as XANES and SIMS analysis of melt inclusions host in the ELIP olivines, is required to better quantify the water content and degree of oxidation. Lower oxygen fugacity and water content in the mantle source would result into a higher potential temperature, but would not affect our conclusion that melting of a relatively homogeneous peridotite mantle source at different P-T conditions can explain the genesis of the ELIP picrites.

Acknowledgments

Claude Herzberg and Jussi S Heinonen are thanked for thorough and critical reviews and suggestions that have greatly improved the quality of the manuscript. The journal editor, Arturo Gomez-Tuena, is thanked for expert editorial handling. We are also grateful to Richard Ernst for language editing and suggestions on an earlier draft. This work was supported by the National Natural Science Foundation of China (41903035 and 41530211), the State Administration of Foreign Expert Affairs of China (the 111 Project: BP0719022), the MOST Special Fund from the State Key Laboratory of Geological Processes and Mineral Resources (CUG, MSFGPMR21 and MSFGPMR01), the China Postdoctoral Science Foundation funded project (2019M652732) and the Fundamental Research Funds for the Central Universities.

Declaration of Competing Interest

None

Appendix A. Supplementary data

Supplementary data to this article can be found online at https://doi.org/10.1016/j.earscirev.2020.103253.

References

Ammannati, E., Jacob, D.E., Avanzinelli, R., Foley, S.F., Conticelli, S., 2016. Low Ni olivine in silica-undersaturated ultrapotassic igneous rocks as evidence for carbonate metasomatism in the mantle. Earth Planet. Sci. Lett. 444, 64–74.

Anderson, D.L., 2005. Large igneous provinces, delamination, and fertile mantle. Elements 1, 271–275.

Asimow, P.D., Langmuir, C.H., 2003. The importance of water to oceanic mantle melting regimes. Nature 421, 815–820.

Bai, Z.-J., Zhong, H., Hu, R.-Z., Zhu, W.-G., Hu, W.-J., 2019. Composition of the chilled marginal rocks of the Panzhihua Layered Intrusion, Emeishan large igneous Province, SW China: implications for parental Magma Compositions, Sulfide Saturation history and Fe–Ti Oxide Mineralization. J. Petrol. 60, 619–648.

Ballard, J.R., Palin, M.J., Campbell, I.H., 2002. Relative oxidation states of magmas inferred from Ce(IV)/Ce(III) in zircon: application to porphyry copper deposits of northern Chile. Contrib. Mineral. Petrol. 144, 347–364.

Balta, J.B., Asimow, P.D., Mosenfelder, J.L., 2011. Manganese partitioning during hydrous melting of peridotite. Geochim. Cosmochim. Acta 75, 5819–5833.

Campbell, I.H., 2007. Testing the plume theory. Chem. Geol. 241, 153–176.

Chung, S.-L., Jahn, B.-M., 1995. Plume-lithosphere interaction in generation of the Emeishan flood basalts at the Permian-Triassic boundary. Geology 23, 889–892.

Davis, F.A., Humayun, M., Hirschmann, M.M., Cooper, R.S., 2013. Experimentally determined mineral/melt partitioning of first-row transition elements (FRTE) during partial melting of peridotite at 3 GPa. Geochim. Cosmochim. Acta 104, 232–260.

De Hoog, J.C.M., Gall, L., Cornell, D.H., 2010. Trace-element geochemistry of mantle olivine and application to mantle petrogenesis and geothermobarometry. Chem. Geol. 270, 196–215.

Ernst, R.E., 2014. Large Igneous Provinces. Cambridge University Press.

Ernst, R.E., Youbi, N., 2017. How large igneous Provinces affect global climate, sometimes cause mass extinctions, and represent natural markers in the geological record. Palaeogeogr. Palaeoclimatol. Palaeoecol. 478, 30–52.

Evans, K.A., Elburg, M.A., Kamenetsky, V.S., 2012. Oxidation state of subarc mantle. Geology 40, 783–786.

Fan, W., Zhang, C., Wang, Y., Guo, F., Peng, T., 2008. Geochronology and geochemistry of Permian basalts in western Guangxi Province, Southwest China: evidence for plume-lithosphere interaction. Lithos 102, 218–236.

Feig, S.T., Koepke, J., Snow, J.E., 2006. Effect of water on tholeiitic basalt phase equilibria: an experimental study under oxidizing conditions. Contrib. Mineral. Petrol. 152, 611–638.

Fitton, J.G., Saunders, A.D., Norry, M.J., Hardarson, B.S., Taylor, R.N., 1997. Thermal and chemical structure of the Iceland plume. Earth Planet. Sci. Lett. 153, 197–208.

Fitton, J.G., Saunders, A.D., Kempton, P.D., Hardarson, B.S., 2003. Does depleted mantle form an intrinsic part of the Iceland plume? Geochem. Geophys. Geosyst. 4 (3), 1032.

Gale, A., Dalton, C.A., Langmuir, C.H., Su, Y., Schilling, J.G., 2013. The mean composition of ocean ridge basalts. Geochem. Geophys. Geosyst. 14, 489–518.

Ganne, J., Feng, X.J., 2017. Primary magmas and mantle temperatures through time. Geochem. Geophy. Geosy. 18, 872–888.

Gao, S., Rudnick, R.L., Xu, W.-L., Yuan, H.-L., Liu, Y.-S., Walker, R.J., Puchtel, I.S., Liu, X., Huang, H., Wang, X.-R., 2008. Recycling deep cratonic lithosphere and generation of intraplate magmatism in the North China Craton. Earth Planet. Sci. Lett. 270, 41–53.

Gavrilenko, M., Herzberg, C., Vidito, C., Carr, M.J., Tenner, T., Ozerov, A., 2016. A Calcium-in-Olivine Geohygrometer and its application to subduction zone magmatism. J. Petrol. 57, 1811–1832.

Hanski, E., Kamenetsky, V.S., Luo, Z.-Y., Xu, Y.-G., Kuzmin, D.V., 2010. Primitive magmas in the Emeishan large Igneous Province, southwestern China and northern Vietnam. Lithos 119, 75–90.

He, B., Xu, Y.-G., Chung, S.-L., Xiao, L., Wang, Y., 2003. Sedimentary evidence for a rapid, kilometer-scale crustal doming prior to the eruption of the Emeishan flood basalts. Earth Planet. Sci. Lett. 213, 391–405.

He, Q., Xiao, L., Balta, B., Gao, R., Chen, J., 2010. Variety and complexity of the Late-Permian Emeishan basalts: reappraisal of plume–lithosphere interaction processes. Lithos 119, 91–107.

Heinonen, J.S., Fusswinkel, T., 2017. High Ni and low Mn/Fe in olivine phenocrysts of the Karoo meimechites do not reflect pyroxenitic mantle sources. Chem. Geol. 467, 134–142.

Heinonen, J.S., Carlson, R.W., Riley, T.R., Luttinen, A.V., Horan, M.F., 2014. Subduction-modified oceanic crust mixed with a depleted mantle reservoir in the sources of the Karoo continental flood basalt province. Earth Planet. Sci. Lett. 394, 229–241.

Herzberg, C., 2011. Identification of source lithology in the Hawaiian and Canary Islands: implications for Origins. J. Petrol. 52, 113–146.

Herzberg, C., Asimow, P.D., 2008. Petrology of some oceanic island basalts: PRIMELT2. XLS software for primary magma calculation. Geochem. Geophys. Geosyst. 9, Q09001.

Herzberg, C., O'Hara, M.J., 2002. Plume-associated ultramafic magmas of Phanerozoic age. J. Petrol. 43, 1857–1883.

Herzberg, C., Asimow, P.D., Arndt, N., Niu, Y., Lesher, C.M., Fitton, J.G., Cheadle, M.J., Saunders, A.D., 2007. Temperatures in ambient mantle and plumes: constraints from basalts, picrites, and komatiites. Geochem. Geophys. Geosyst. 8, Q02006.

Herzberg, C., Asimow, P.D., Ionov, D.A., Vidito, C., Jackson, M.G., Geist, D., 2013. Nickel and helium evidence for melt above the core–mantle boundary. Nature 493, 393–397.

Hirschmann, M.M., 2000. Mantle solidus: Experimental constraints and the effects of peridotite composition. Geochem. Geophy. Geosy. 1, 2000GC000070.

Hirschmann, M.M., Kogiso, T., Baker, M.B., Stolper, E.M., 2003. Alkalic magmas generated by partial melting of garnet pyroxenite. Geology 31, 481–484.

Howarth, G.H., Harris, C., 2017. Discriminating between pyroxenite and peridotite sources for continental flood basalts (CFB) in southern Africa using olivine chemistry. Earth Planet. Sci. Lett. 475, 143–151.

Husen, A., Almeev, R.R., Holtz, F., 2016. The effect of H2O and pressure on Multiple Saturation and liquid Lines of Descent in Basalt from the Shatsky rise. J. Petrol. 57, 309–344.

Imai, A., Listanco, E., Fujii, T., 1993. Petrologic and sulfur isotopic significance of highly oxidized and sulfur-rich magma of Mt. Pinatubo, Philippines. Geology 21, 699–702.

Ivanov, A.V., Mukasa, S.B., Kamenetsky, V.S., Ackerson, M., Demonterova, E.I., Pokrovsky, B.G., Vladykin, N.V., Kolesnichenko, M.V., Litasov, K.D., Zedgenizov, D.A., 2018. Volatile concentrations in olivine-hosted melt inclusions from meimechite and melanephelinite lavas of the Siberian Traps large Igneous Province: evidence for flux-related high-Ti, high-Mg magmatism. Chem. Geol. 483, 442–462.

Jiang, Q., Qiu, N., Zhu, C., 2018. Heat flow study of the Emeishan large igneous province region: Implications for the geodynamics of the Emeishan mantle plume. Tectonophysics 724-725, 11–27.

Kamenetsky, V.S., Chung, S.L., Kamenetsky, M.B., Kuzmin, D.V., 2012. Picrites from the

Emeishan large Igneous Province, SW China: a Compositional Continuum in Primitive Magmas and their Respective Mantle sources. J. Petrol. 53, 2095–2113.

Katz, R.F., Spiegelman, M., Langmuir, C.H., 2003. A new parameterization of hydrous mantle melting. Geochem. Geophy. Geosy. 4 (9), 1073.

Kelley, K.A., Cottrell, E., 2009. Water and the oxidation state of subduction zone magmas. Science 325, 605–607.

Kelley, K.A., Plank, T., Grove, T.L., Stolper, E.M., Newman, S., Hauri, E., 2006. Mantle melting as a function of water content beneath back-arc basins. J. Geophys. Res. 111, B09208.

Kelley, K.A., Plank, T., Newman, S., Stolper, E.M., Grove, T.L., Parman, S., Hauri, E.H., 2010. Mantle melting as a function of water content beneath the Mariana Arc. J. Petrol. 51, 1711–1738.

Kogiso, T., 2004. High-pressure partial melting of Mafic Lithologies in the Mantle. J. Petrol. 45, 2407–2422.

Kress, V.C., Carmichael, I.S., 1991. The compressibility of silicate liquids containing Fe_2O_3 and the effect of composition, temperature, oxygen fugacity and pressure on their redox states. Contrib. Mineral. Petrol. 108, 82–92 Springer.

Lambart, S., 2017. No direct contribution of recycled crust in Icelandic basalts. Geochem. Perspect. Lett. 4, 7–12.

Lambart, S., Laporte, D., Schiano, P., 2013. Markers of the pyroxenite contribution in the major-element compositions of oceanic basalts: Review of the experimental constraints. Lithos 160-161, 14–36.

Lambart, S., Baker, M.B., Stolper, E.M., 2016. The role of pyroxenite in basalt genesis: Melt-PX, a melting parameterization for mantle pyroxenites between 0.9 and 5 GPa. J. Geophys. Res. Solid Earth 121, 5708–5735.

Le Roux, V., Dasgupta, R., Lee, C.T., 2011. Mineralogical heterogeneities in the Earth's mantle: Constraints from Mn, Co, Ni and Zn partitioning during partial melting. Earth Planet. Sci. Lett. 307, 395–408.

Lee, C.-T.A., Luffi, P., Plank, T., Dalton, H., Leeman, W.P., 2009. Constraints on the depths and temperatures of basaltic magma generation on Earth and other terrestrial planets using new thermobarometers for mafic magmas. Earth Planet. Sci. Lett. 279, 20–33.

Li, J., Xu, J.F., Suzuki, K., He, B., Xu, Y.G., Ren, Z.Y., 2010. Os, Nd and Sr isotope and trace element geochemistry of the Muli picrites: Insights into the mantle source of the Emeishan large Igneous Province. Lithos 119, 108–122.

Li, C., Tao, Y., Qi, L., Ripley, E.M., 2012. Controls on PGE fractionation in the Emeishan picrites and basalts: Constraints from integrated lithophile–siderophile elements and Sr–Nd isotopes. Geochim. Cosmochim. Acta 90, 12–32.

Li, J., Wang, X.-C., Ren, Z.-Y., Xu, J.-F., He, B., Xu, Y.-G., 2014. Chemical heterogeneity of the Emeishan mantle plume: evidence from highly siderophile element abundances in picrites. J. Asian Earth Sci. 79, 191–205.

Li, H., Zhang, Z., Ernst, R., Lü, L., Santosh, M., Zhang, D., Cheng, Z., 2015. Giant radiating mafic dyke swarm of the Emeishan large Igneous Province: Identifying the mantle plume Centre. Terra Nova 27, 247–257.

Liu, J., Xia, Q.K., Kuritani, T., Hanski, E., Yu, H.R., 2017. Mantle hydration and the role of water in the generation of large igneous provinces. Nat. Commun. 8, 1824.

Matzen, A.K., Baker, M.B., Beckett, J.R., Stolper, E.M., 2011. Fe–Mg partitioning between olivine and high-magnesian melts and the nature of Hawaiian parental liquids. J. Petrol. 52, 1243–1263.

Matzen, A.K., Baker, M.B., Beckett, J.R., Stolper, E.M., 2013. The Temperature and pressure Dependence of Nickel Partitioning between Olivine and Silicate Melt. J. Petrol. 54, 2521–2545.

Matzen, A.K., Baker, M.B., Beckett, J.R., Wood, B.J., Stolper, E.M., 2017a. The effect of liquid composition on the partitioning of Ni between olivine and silicate melt. Contrib. Mineral. Petrol. 172, 3.

Matzen, A.K., Wood, B.J., Baker, M.B., Stolper, E.M., 2017b. The roles of pyroxenite and peridotite in the mantle sources of oceanic basalts. Nat. Geosci. 10, 530–535.

Mironov, N.L., Portnyagin, M.V., 2011. H_2O and CO_2 in parental magmas of Kliuchevskoi volcano inferred from study of melt and fluid inclusions in olivine. Russ. Geol. Geophys. 52, 1353–1367.

Moussallam, Y., Longpré, M.-A., McCammon, C., Gomez-Ulla, A., Rose-Koga, E.F., Scaillet, B., Peters, N., Gennaro, E., Paris, R., Oppenheimer, C., 2019. Mantle plumes are oxidised. Earth Planet. Sci. Lett. 527, 115798.

Mysen, B.O., Dubinsky, E.V., 2004. Melt structural control on olivine/melt element partitioning of ca and Mn. Geochim. Cosmochim. Acta 68, 1617–1633.

Niu, Y., Wilson, M., Humphreys, E.R., O'Hara, M.J., 2011. The Origin of Intra-plate Ocean Island Basalts (OIB): the Lid effect and its Geodynamic Implications. J. Petrol. 52, 1443–1468.

Parman, S.W., Grove, T.L., Kelley, K.A., Plank, T., 2011. Along-Arc Variations in the Pre-Eruptive H_2O Contents of Mariana Arc Magmas Inferred from Fractionation Paths. J. Petrol. 52, 257–278.

Putirka, K.D., 2005. Mantle potential temperatures at Hawaii, Iceland, and the mid-ocean ridge system, as inferred from olivine phenocrysts: evidence for thermally driven mantle plumes. Geochem. Geophys. Geosyst. 6, Q05L08.

Putirka, K.D., 2008. Thermometers and barometers for volcanic systems. Rev. Mineral. Geochem. 69, 61–120.

Putirka, K., Ryerson, F.J., Perfit, M., Ridley, W.I., 2011. Mineralogy and composition of the oceanic mantle. J. Petrol. 52, 279–313.

Putirka, K., Tao, Y., Hari, K.R., Perfit, M.R., Jackson, M.G., Arevalo, R., 2018. The mantle source of thermal plumes: trace and minor elements in olivine and major oxides of primitive liquids (and why the olivine compositions don't matter). Am. Mineral. 103, 1253–1270.

Ren, Z.-Y., Wu, Y.-D., Zhang, L., Nichols, A.R.L., Hong, L.-B., Zhang, Y.-H., Zhang, Y., Liu, J.-Q., Xu, Y.-G., 2017. Primary magmas and mantle sources of Emeishan basalts constrained from major element, trace element and Pb isotope compositions of olivine-hosted melt inclusions. Geochim. Cosmochim. Acta 208, 63–85.

Roeder, P.L., Emslie, R., 1970. Olivine-liquid equilibrium. Contrib. Mineral. Petrol. 29, 275–289.

Shellnutt, J.G., 2014. The Emeishan large igneous province: a synthesis. Geosci. Front. 5, 369–394.

Shellnutt, J.G., Pham, T.T., 2018. Mantle potential temperature estimates and primary melt compositions of the Low-Ti Emeishan Flood Basalt. Front. Earth Sci. 6, 67.

Sobolev, A.V., Hofmann, A.W., Kuzmin, D.V., Yaxley, G.M., Arndt, N.T., Chung, S.-L., Danyushevsky, L.V., Elliott, T., Frey, F.A., Garcia, M.O., 2007. The amount of recycled crust in sources of mantle-derived melts. Science 316, 412–417.

Sobolev, A.V., Sobolev, S.V., Kuzmin, D.V., Malitch, K.N., Petrunin, A.G., 2009. Siberian meimechites: origin and relation to flood basalts and kimberlites. Russ. Geol. Geophys. 50, 999–1033.

Song, X.Y., Zhou, M.F., Hou, Z.Q., Cao, Z.M., Wang, Y.L., Li, Y.G., 2001. Geochemical constraints on the mantle source of the upper permian Emeishan continental flood basalts, southwestern China. Int. Geol. Rev. 43, 213–225.

Stolper, E., Asimow, P., 2007. Insights into mantle melting from graphical analysis of one-component systems. Am. J. Sci. 307, 1051–1139.

Sun, S.S., McDonough, W.F., 1989. Chemical and isotopic systematics of oceanic basalts: implications for mantle composition and processes. Geol. Soc. Lond., Spec. Publ. 42, 313–345.

Sun, W.-D., Liang, H.-Y., Ling, M.-X., Zhan, M.-Z., Ding, X., Zhang, H., Yang, X.-Y., Li, Y.-L., Ireland, T.R., Wei, Q.-R., 2013. The link between reduced porphyry copper deposits and oxidized magmas. Geochim. Cosmochim. Acta 103, 263–275.

Tao, Y., Putirka, K., Hu, R.-Z., Li, C., 2015. The magma plumbing system of the Emeishan large igneous province and its role in basaltic magma differentiation in a continental setting. Am. Mineral. 100, 2509–2517.

Till, C.B., Grove, T.L., Krawczynski, M.J., 2012. A melting model for variably depleted and enriched lherzolite in the plagioclase and spinel stability fields. J. Geophys. Res. Solid Earth 117, B06206 (n/a-n/a).

Turner, S., Hawkesworth, C., 1995. The nature of the sub-continental mantle: constraints from the major-element composition of continental flood basalts. Chem. Geol. 120, 295–314.

Ukstins-Peate, I., Bryan, S.E., 2008. Re-evaluating plume-induced uplift in the Emeishan large igneous province. Nat. Geosci. 1, 625–629.

Villiger, S., 2004. The liquid line of descent of anhydrous, mantle-derived, tholeiitic liquids by fractional and equilibrium crystallization–an experimental study at 1.0 GPa. J. Petrol. 45, 2369–2388.

Villiger, S., Ulmer, P., Muntener, O., 2007. Equilibrium and fractional crystallization experiments at 0.7 GPa; the effect of pressure on phase relations and liquid compositions of tholeiitic magmas. J. Petrol. 48, 159–184.

Wade, J.A., Plank, T., Hauri, E.H., Kelley, K.A., Roggensack, K., Zimmer, M., 2008. Prediction of magmatic water contents via measurement of H_2O in clinopyroxene phenocrysts. Geology 36, 799–802.

Wang, C.Y., Zhou, M.F., Qi, L., 2007. Permian flood basalts and mafic intrusions in the Jinping (SW China) Song Da (northern Vietnam) district: Mantle sources, crustal contamination and sulfide segregation. Chem. Geol. 243, 317–343.

Wang, X.-C., Wilde, S.A., Xu, B., Pang, C.-J., 2016. Origin of arc-like continental basalts: implications for deep-Earth fluid cycling and tectonic discrimination. Lithos 261, 5–45.

Wu, Y.-D., Ren, Z.-Y., Handler, M.R., Zhang, L., Qian, S.-P., Xu, Y.-G., Wang, C.Y., Wang, Y., Chen, L.-L., 2018. Melt diversity and magmatic evolution in the Dali picrites, Emeishan large igneous Province. J. Geophys. Res. Solid Earth 123, 9635–9657.

Xiao, L., Xu, Y.G., Mei, H.J., Zheng, Y.F., He, B., Pirajno, F., 2004. Distinct mantle sources of low-Ti and high-Ti basalts from the western Emeishan large igneous province, SW China: implications for plume–lithosphere interaction. Earth Planet. Sci. Lett. 228, 525–546.

Xu, R., Liu, Y., 2016. Al-in-olivine thermometry evidence for the mantle plume origin of the Emeishan large igneous province. Lithos 266-267, 362–366.

Xu, Y., Chung, S.-L., Jahn, B.-m., Wu, G., 2001. Petrologic and geochemical constraints on the petrogenesis of Permian–Triassic Emeishan flood basalts in southwestern China. Lithos 58, 145–168.

Xu, Y.-G., He, B., Chung, S.-L., Menzies, M.A., Frey, F.A., 2004. Geologic, geochemical, and geophysical consequences of plume involvement in the Emeishan flood-basalt province. Geology 32, 917–920.

Yang, C., Liu, S.A., 2019. Zinc Isotope Constraints on Recycled Oceanic Crust in the Mantle sources of the Emeishan large Igneous Province. J. Geophys. Res. Solid Earth 124, 12537–12555.

Yang, Z.-F., Zhou, J.-H., 2013. Can we identify source lithology of basalt? Sci. Rep. 3.

Yang, Z.-F., Li, J., Liang, W.-F., Luo, Z.-H., 2016. On the chemical markers of pyroxenite contributions in continental basalts in Eastern China: implications for source lithology and the origin of basalts. Earth Sci. Rev. 157, 18–31.

Yao, J.-H., Zhu, W.-G., Li, C., Zhong, H., Yu, S., Ripley, E.M., Bai, Z.-J., 2019. Olivine O isotope and trace element constraints on source variation of picrites in the Emeishan flood basalt province, SW China. Lithos 338-339, 87–98.

Yu, S.-Y., Shen, N.-P., Song, X.-Y., Ripley, E.M., Li, C., Chen, L.-M., 2017. An integrated chemical and oxygen isotopic study of primitive olivine grains in picrites from the Emeishan large Igneous Province, SW China: evidence for oxygen isotope heterogeneity in mantle sources. Geochim. Cosmochim. Acta 215, 263–276.

Zamboni, D., Trela, J., Gazel, E., Sobolev, A.V., Cannatelli, C., Lucchi, F., Batanova, V.G., De Vivo, B., 2017. New insights into the Aeolian Islands and other arc source compositions from high-precision olivine chemistry. Lithos 272-273, 185–191.

Zhang, Z., Mahoney, J.J., Mao, J., Wang, F., 2006. Geochemistry of picritic and associated basalt flows of the western Emeishan flood basalt province, China. J. Petrol. 47, 1997–2019.

Zhang, Z., Zhi, X., Chen, L., Saunders, A.D., Reichow, M.K., 2008. Re–Os isotopic compositions of picrites from the Emeishan flood basalt province, China. Earth Planet. Sci. Lett. 276, 30–39.

Zhang, L., Ren, Z.-Y., Handler, M.R., Wu, Y.-D., Zhang, L., Qian, S.-P., Xia, X.-P., Yang, Q., Xu, Y.-G., 2019. The origins of high-Ti and low-Ti magmas in large igneous provinces, insights from melt inclusion trace elements and Sr-Pb isotopes in the Emeishan large Igneous Province. Lithos 344-345, 122–133.

Zhong, Y.-T., He, B., Mundil, R., Xu, Y.-G., 2014. CA-TIMS zircon U–Pb dating of felsic ignimbrite from the Binchuan section: Implications for the termination age of Emeishan large igneous province. Lithos 204, 14–19.

Zhu, J., Zhang, Z., Reichow, M.K., Li, H., Cai, W., Pan, R., 2018. Weak Vertical Surface Movement Caused by the Ascent of the Emeishan Mantle Anomaly. J. Geophys. Res. Solid Earth 123, 1018–1034.